Supporting Information for Quantum Embedding Theory for Strongly-correlated States in Materials

He Ma,[†] Nan Sheng,[†] Marco Govoni,[*,‡,¶] and Giulia Galli[*,‡,†,¶]

†*Department of Chemistry, University of Chicago, Chicago, IL 60637, USA.*

‡*Pritzker School of Molecular Engineering, University of Chicago, Chicago, IL 60637, USA.*

¶*Materials Science Division and Center for Molecular Engineering, Argonne National Laboratory, Lemont, IL 60439, USA.*

E-mail: mgovoni@anl.gov; gagalli@uchicago.edu

1 Evaluation of matrix elements of screened Coulomb interaction

The polarization component of screened Coulomb interaction can be written as $w\chi^{\mathrm{E}}w$, where $w \in \{v, f_{\mathrm{Hxc}}\}$, $\chi^{\mathrm{E}} \in \{\chi^{\mathrm{E}}_{\mathrm{rpa}}, \chi^{\mathrm{E}}_{\mathrm{tc}}, \chi^{\mathrm{E}}_{\mathrm{el}}, \chi^{\mathrm{E}}_{\mathrm{vel}}\}$. Under these notations, the polarization part of W^{E} can be computed as

$$[ij|w\chi^{\mathrm{E}}w|kl] = \tilde{\chi}^{\mathrm{E}}_{00}\delta_{ij}\delta_{kl}\left(\int_{\mathrm{BZ}}\frac{d\boldsymbol{q}}{(2\pi)^3}v(q)\right) + \frac{1}{\Omega}\sum_{m,n}^{N_{\mathrm{PDEP}}}\langle\rho_{ij}v^{1/2}|\varphi_m\rangle\,[\tilde{w}\tilde{\chi}^{\mathrm{E}}\tilde{w}]_{mn}\,\langle\varphi_n|v^{1/2}\rho_{kl}\rangle \tag{1}$$

where the first term stems from the macroscopic (head) part of polarizability and involves an integration over the first brillioun zone; $\tilde{\chi}^{\mathrm{E}}_{00}$ denotes the head of $\tilde{\chi}^{\mathrm{E}}$; δ is the Kronecker delta; v denotes the bare Coulomb interaction. The second term in the r.h.s. of Eq. 1 stems from the microscopic (body) part of polarizability, with Ω being the volume of the periodic cell. In Eq. 1 we have utilized a resolution-of-identity (RI) expression for the microscopic part on the PDEP basis, where

$$\langle\rho_{ij}v^{1/2}|\varphi_m\rangle = \sum_{\boldsymbol{G}\neq 0}(\zeta_i\zeta_j)(\boldsymbol{G})^* v^{1/2}(\boldsymbol{G})\varphi_m(\boldsymbol{G}) \tag{2}$$

is the overlap integrals between products of ζ and PDEP basis, and $\tilde{w}\tilde{\chi}^{\mathrm{E}}\tilde{w}$ represents matrix multiplications between $\tilde{w}$ and $\tilde{\chi}^{\mathrm{E}}$ in the PDEP basis.

2 Convergence tests for the parameter N_{PDEP}

In order to assess the numerical robustness of evaluating density response functions in the PDEP basis, in Fig. S1 we present the excitation energies of the NV center as functions of N_{PDEP}, the parameter that controls the numerical accuracy of response functions and the RI approximation to the matrix elements of W^{E}. We see that as N_{PDEP} increase, the excitation energies of NV rapidly converge. When $N_{\mathrm{PDEP}} = 512$, the excitation energies have converged within 0.01 eV.

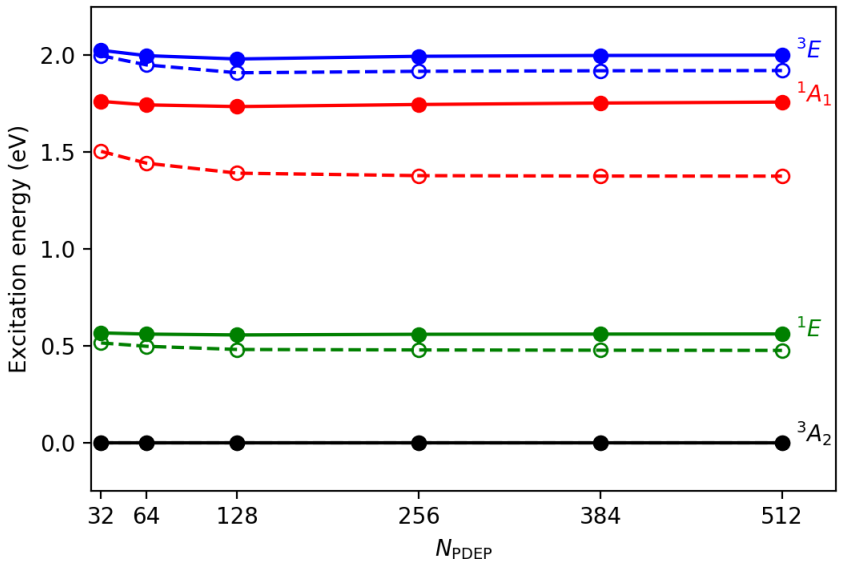

Figure S1: Vertical excitation energies of NV center in diamond as functions of N_{PDEP} parameter (see text). Dashed and solid lines represent excitation energies obtained within ($W^{\mathrm{E}}_{\mathrm{rpa}}$) and beyond ($W^{\mathrm{E}}_{\mathrm{vel}}$) the RPA, respectively.

Similarly to the calculations of excitation energies of spin-defects, we found that the predicted Hubbard parameters of $SrTiO_3$ rapidly converged as a function of the size of the PDEP basis (Fig. S2). When $N_{\mathrm{PDEP}} = 512$, the Hubbard parameters have converged within 0.02 eV.

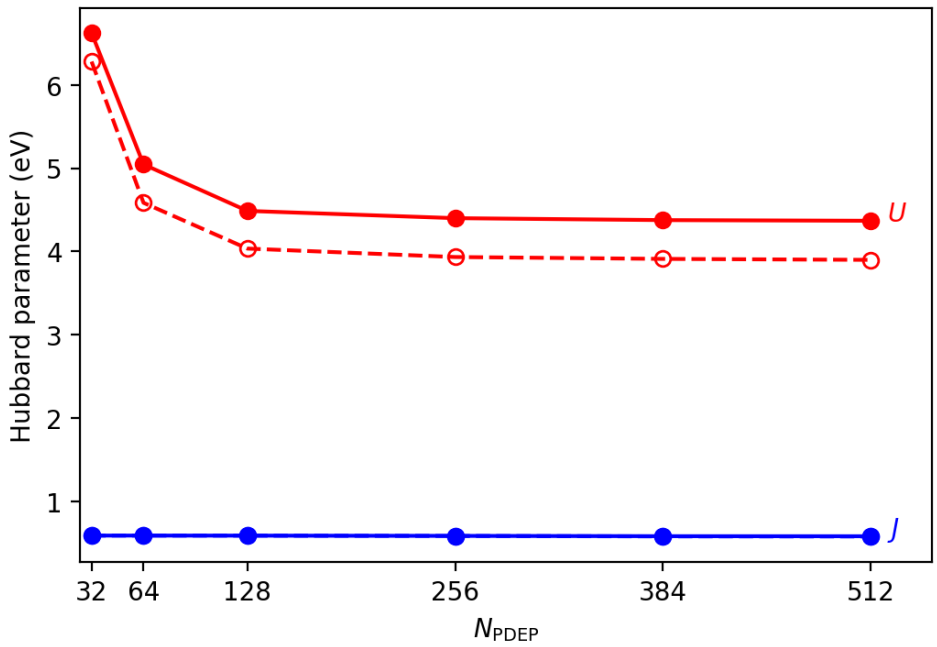

Figure S2: Hubbard parameters U and J of $SrTiO_3$ as functions of N_{PDEP} (see text). Dashed and solid lines represent Hubbard parameters obtained within ($W^{\mathrm{E}}_{\mathrm{rpa}}$) and beyond ($W^{\mathrm{E}}_{\mathrm{vel}}$) the RPA, respectively.

3 Convergence tests for the size of active space

In order to assess the influence of the size of active space in the current theoretical framework, in Fig. S3 we present the excitation energies of the NV center as functions of the size of the active space. We see that as the size of the active space increases, the excitation energies have converged within 0.01 eV.

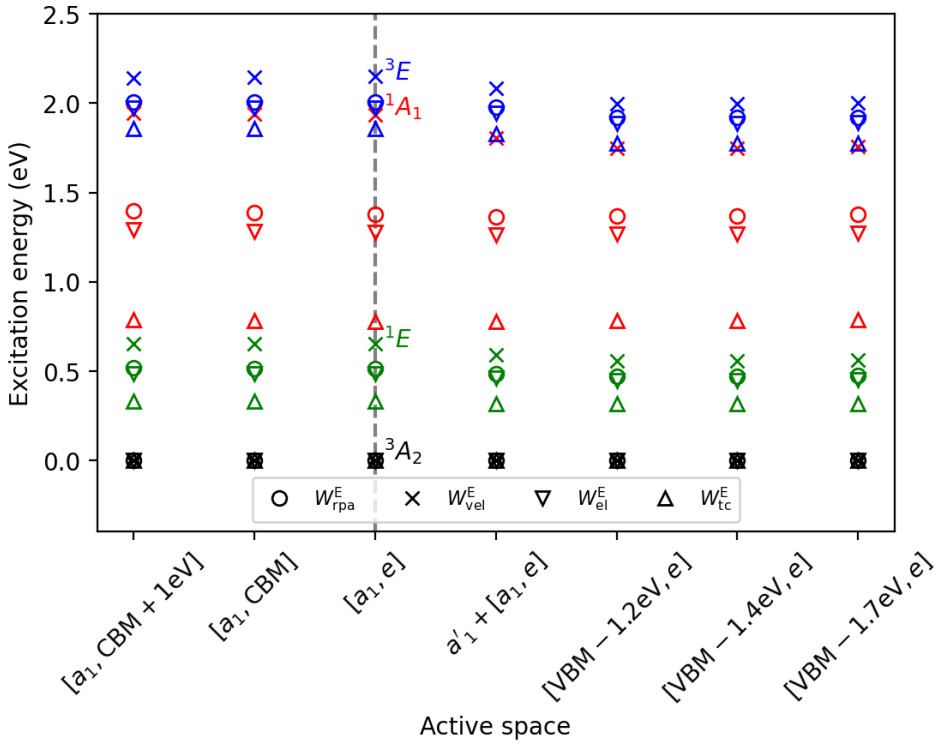

Figure S3: Vertical excitation energies of NV center in diamond as functions of the size of active space (see text). The set [a_1, e] represents a minimum model of NV composed of only a_1 and e defect orbitals; the set [a_1, CBM + 1eV] includes the a1 defect orbital and conduction orbitals between the conduction band minimum (CBM) and 1 eV above the CBM; the set [VBM - 1.7eV, e] includes the e defect orbital and valence orbitals between the valence band maximum (VBM) and 1.7 eV below the VBM. Circles, crosses and upper and lower triangles represent different definitions of screened Coulomb interactions, as indicated in the inset of the figure; different colors represent different excited states.

4 Test for unscreened Coulomb interaction

In order to demonstrate the importance of the screening part in screened Coulomb interaction, in Tab. S1 we report results obtained with both unscreened interactions and screened interactions, and experimental references for the NV center. The unscreened interactions lead to unphysical results for excitation energies, which are very different from the experimental values.

Table S1: Vertical excitation energies (eV) of spin-defects including the negatively-charged nitrogen-vacancy (NV), neutral silicon-vacancy (SiV), dicancy (VV) and Cr center in diamond. Calculations are performed using the bare Coulomb interaction V_{bare} and partially screened Coulomb interaction W_{vel} as the interaction in the effective Hamiltonian. Reference vertical excitation energies are computed from experimental zero-phonon lines (ZPL) when Stokes energies are available. Reference experimental values for ZPLs are shown in brackets in the last column.

		PBE		DDH		Ref
		V_{bare}	$W^{\text{E}}_{\text{vel}}$	V_{bare}	$W^{\text{E}}_{\text{vel}}$	
System	Excitation					
NV	${}^3E \leftrightarrow {}^3A_2$	-0.089	1.458	0.513	2.001	2.180 (1.945)
	${}^1A_1 \leftrightarrow {}^3A_2$	0.042	1.437	0.901	1.759	
	${}^1E \leftrightarrow {}^3A_2$	0.015	0.444	0.245	0.561	
	${}^1A_1 \leftrightarrow {}^1E$	0.028	0.993	0.656	1.198	(1.190)
	${}^3E \leftrightarrow {}^1A_1$	-0.131	0.020	-0.388	0.243	(0.344-0.430)
SiV	${}^3E_u \leftrightarrow {}^3A_{2g}$	-0.111	1.258	0.166	1.594	1.568 (1.31)
	${}^3A_{1u} \leftrightarrow {}^3A_{2g}$	0.326	1.416	0.697	1.792	
	${}^1E_g \leftrightarrow {}^3A_{2g}$	-0.038	0.281	0.193	0.336	
	${}^1A_{1g} \leftrightarrow {}^3A_{2g}$	-0.110	0.478	0.210	0.583	
	${}^1A_{1u} \leftrightarrow {}^3A_{2g}$	0.080	1.277	0.354	1.623	
	${}^3E_u \leftrightarrow {}^3A_{2u}$	0.149	0.002	0.144	0.011	(0.007)
VV	${}^3E \leftrightarrow {}^3A_2$	-0.282	0.985	0.050	1.270	(1.095)
	${}^1A_1 \leftrightarrow {}^3A_2$	-0.377	0.908	0.125	1.156	
	${}^1E \leftrightarrow {}^3A_2$	-0.082	0.274	0.045	0.348	
	${}^1A_1 \leftrightarrow {}^1E$	-0.296	0.634	0.079	0.808	
	${}^3E \leftrightarrow {}^1A_1$	0.096	0.077	-0.075	0.114	
Cr	${}^3E \leftrightarrow {}^3A_2$	-0.093	0.890	-0.072	1.343	
	${}^3A_1 \leftrightarrow {}^3A_2$	0.966	0.956	0.343	1.394	
	${}^3E' \leftrightarrow {}^3A_2$	0.941	1.189	0.352	1.744	
	${}^3A'_2 \leftrightarrow {}^3A_2$	1.497	1.237	0.864	1.783	
	${}^1E \leftrightarrow {}^3A_2$	0.287	1.017	0.314	1.130	(1.190)
	${}^1A_1 \leftrightarrow {}^3A_2$	0.601	1.566	0.647	2.013	

5 Maximally localized Wannier functions of $SrTiO_3$

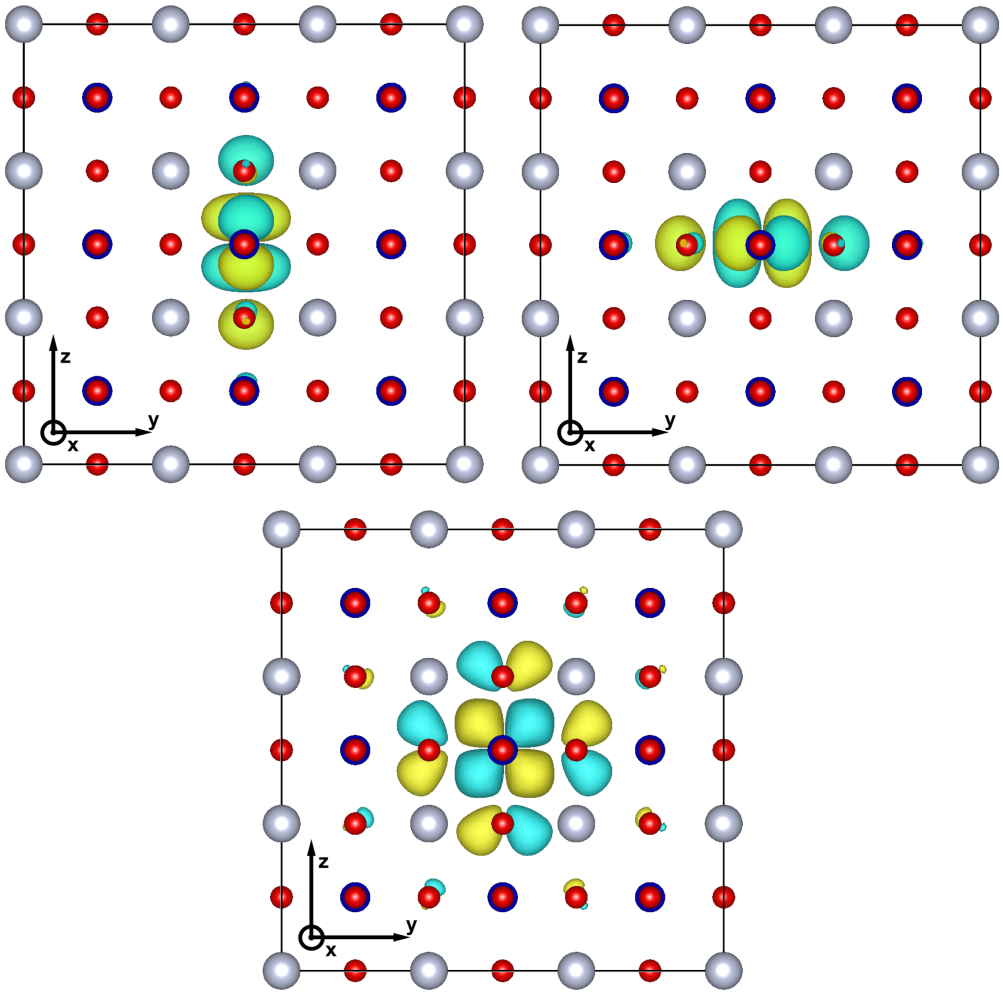

Figure S4: Three MLWFs built from t_{2g} bands of $SrTiO_3$. Ti, Sr and O atoms are colored by blue, grey and red, respectively.

Data that support the findings of this study are available through Qresp[1] at `https://paperstack.uchicago.edu/paperdetails/603d32f0057dbbfb35b05d4d?server=https%3A%2F%2Fpaperstack.uchicago.edu`

References

(1) Govoni, M.; Munakami, M.; Tanikanti, A.; Skone, J. H.; Runesha, H. B.; Giberti, F.; de Pablo, J.; Galli, G. Qresp, a tool for curating, discovering and exploring reproducible scientific papers. *Sci. Data* **2019**, *6*, 190002.